Proceedings of 2022 IEEE
International Conference on Mechatronics and Automation
August 7 - 10, Guilin, China

Comparison of Spherical and Fish-shaped Robots on Hydrodynamic and Pressure Characteristics in Static Water

Ao Li[1], Shuxiang Guo[1], Liwei Shi[1], Meng Liu1, Mugen Zhou[1], He Yin[1]*

1 Key Laboratory of Convergence Medical Engineering System and Healthcare Technology, the Ministry of Industry and Information Technology, School of Life Science, Beijing Institute of Technology, No.5, Zhongguancun South Street, Haidian District, Beijing 100081, China

{ liao & guoshuxiang & shiliwei } @bit.edu.cn;

* Corresponding author

***Abstract* - During the underwater movement of underwater robot, a large part of interference comes from the interaction between robot and water flow. In order to control the underwater robot accurately, it is very important to study the hydrodynamic characteristics of the robot. In this paper, the hydrodynamic characteristics about two kinds of underwater robots (spherical and fish-shaped robot) are studied according the application. Firstly, the hydrodynamic characteristics of the two shapes are studied by the qualitative analysis of velocity field and pressure field. Then, by changing the speed and volume of the robot, the drag resistance force of the robot is further quantitatively analyzed. These obtained characteristics can be used to guide the application of flow rate sensing and pressure sensing on underwater robots.**

Index Terms - Underwater spherical robot, Underwater fish-shaped robot, Computational Fluid Dynamic, Pressure sensing.

I. INTRODUCTION

Underwater vehicles are important carriers for people to explore the ocean. It includes some large underwater vessels and some small underwater robots. They come in different shapes and sizes, and are used in different fields and roles. The small underwater vehicles or robots may be generally used for ocean exploration, oceanographic sampling, pipeline and cable inspection, search and probe etc [1-3]. Due to the need of detection, the design of the vehicle pays more attention to small size, flexible movement and sensitive environmental perception [4]. In this way, during the exploration process, the robot can not only carry out the exploration in the wide water, but also go deep into some narrow areas [5]. In addition, in recent years, more and more attention has been paid to the research on artificial lateral line of small underwater robots [6]. The research of artificial lateral line will also enhance the ability of environment perception, anti-interference and adaptability to dark underwater environment of underwater vehicles [7].

Underwater vehicles are covered by an envelope called a hydrodynamic hull, forming a free stream body [8]. The hydrodynamic performance of the body determines the performance of underwater vehicle [9]. Therefore, good shape design of underwater vehicle is very important for underwater robot. In terms of optimizing hull shape, most researchers focus on reducing drag [10]. There has been a lot of research on drag reduction. In some hull designs, axisymmetric bodies based on optimization procedures are used to minimize drag [11]. However, some researchers showed that the traditional design did not have the least drag when wave making resistance existed [12]. In addition to drag, other hydrodynamic characteristics can also affect AUV performance, including fluid pressure distribution around the hull, changes in the added mass of the hull, and the effect of body form on maneuverability or hydrodynamic damping derivative [13]. The body shape design should consider various hydrodynamic influences comprehensively and combine with the function of the vehicle itself [14].

At present, computational fluid dynamics (CFD) has become an important analysis, research and design tool of underwater vehicle, especially in the aspects of resistance, propeller performance, maneuverability and so on by simulating [15]. In most experiments, the determination of hydrodynamic characteristics depends on hydrodynamic coefficient [16]. These coefficients were calculated as follows: first, let the fluid flow through the vehicles at a certain linear or angular velocity in a numerical environment to determine the hydrodynamic force and torque acting on the object; then, the hydrodynamic stability criterion can be expressed by the hydrodynamic coefficient calculated by CFD to measure the stability of the required hull [17]. However, this kind of method has significant limitations. On the one hand, it cannot simulate the actual motion of the hull [18]. On the other hand, a lot of information about the flow field during motion of hull was discarded, only part of the motion coefficient was obtained, and the hydrodynamic characteristics of the hull could not be comprehensively analyzed [19].

Based on the situation that the hydrodynamic parameters are single and the simulation is not realistic, this paper proposed a method based on dynamic water environment simulation to analyze the flow field of two common forms of small underwater robot. These two forms are spherical robot and fish-shaped robot. The data of the flow field, such as pressure and velocity, are comprehensively analyzed to clarify the hydrodynamic characteristics of the two types of robots. In part Ⅱ, the dynamic water environment simulation method -- immersed boundary lattice Boltzmann method and the simulation setting are briefly introduced. In part Ⅲ, the robot movement under different conditions are simulated, and the

hydrodynamic characteristics of two types of robots are analyzed. The summary is in part Ⅳ.

II. Method and Modeling

A. Numerical Method

Numerical simulation is widely used in the calculation of hydrodynamic coefficients of underwater vehicles instead of underwater robot pool test. The numerical method has the advantages of not being affected by the accuracy of test equipment and low cost. In addition, this method can provide an ideal simulation environment and quantitatively control the existence and type of interference. Based on lattice Boltzmann method (LBM), the flow field and motion characteristics of robot unsteady motion can be calculated quickly and accurately. LBM method obtains macroscopic fluid motion law through statistics of microscopic particles of discrete fluid. The lattice Boltzmann method based on immersed boundary method can realize unsteady simulation without complicated meshwork.

Boltzmann equation describes the evolution of distribution function $f_i(\boldsymbol{r},t)$. For the discrete solution of continuous Boltzmann equation, its discrete equation [20] is defined as follows:

$$f_i(\boldsymbol{r}+c_i\Delta t,t+\Delta t)=f_i(\boldsymbol{r},t)+\Omega_i^B \tag{1}$$

where, i is the number of particle movement direction, i = 1, 2, …, b. D3Q18 model was adopted in this paper, b =18. f_i is the distribution function of i direction; r is the position vector in the lattice; c_i is the streaming velocity; t is discrete time; Δt is the time step; Ω_i^B is the collision term.

The most widely used lattice Boltzmann-BGK (LBGK) model is adopted as collision term, and its evolution equation is as follows [21] :

$$f_i'(\boldsymbol{r},t)=f_i(\boldsymbol{r},t)-\frac{1}{\tau}\left(f_i(\boldsymbol{r},t)-{f_i}^{eq}(\boldsymbol{r},t)\right) \tag{2}$$

${f_i}^{eq}$ is the local equilibrium distribution function in the *i* direction. τ is the relaxation time

$${f_i}^{eq}(\boldsymbol{r},t)=\omega_i\rho\left(1+\frac{3c_iu}{c_s^2}+\frac{9(c_iu)^2}{c_s^2}-\frac{3u^2}{2c_s^2}\right) \tag{3}$$

where, ω_i is the weight coefficient of lattice vector; ρ is fluid density; u is the average fluid velocity; c_s is sound speed of in fluid. Collision step and streaming step are two important steps of LBM method. The collision step is shown in Formula 1, and the streaming step is calculated by the following formula:

$$f_i(\boldsymbol{r}+c_i\Delta t,t+\Delta t)=f_i'(\boldsymbol{r},t) \tag{4}$$

On the basis of lattice Boltzmann method, multi-direct force immersion boundary method is used to deal with the moving boundary. The immersed boundary method uses fixed Cartesian coordinates to describe the fluid and discrete Lagrange points to describe the moving boundary. It is assumed that the fluid velocity of the flow field at n+1 time level is u_1^{n+1}, and subscript 1 represents the first iteration. Then the velocity of Lagrange point *k* can be expressed as:

$$\hat{\mathrm{u}}_k^1=\sum u_1^{n+1}\cdot\delta(x_k-x)\cdot h^2 \tag{5}$$

$\hat{\mathrm{u}}_k^1$ can be used as the velocity of the Lagrange point, but the no-slip condition is not satisfied. h is the mesh size of flow field. In order to make the moving boundary reach the no-slip condition, the direct force can be further iterated by:

$$F_k^2(x_k)=\frac{u_p-\hat{\mathrm{u}}_k^1}{\Delta t} \tag{6}$$

Then, the forces at the Lagrange points are dispersed into the Eulerian coordinate system:

$$f^2=\sum F_k^2(x_k)\ \delta(x_k-x)\cdot ds \tag{7}$$

$$\delta(x_k-x)=\frac{1}{h^2}d_h\left(\frac{x_k-x}{h}\right)d_h\left(\frac{y_k-y}{h}\right) \tag{8}$$

h is the Eulerian mesh size, and

$$d_h\left(\frac{x_k-x}{h}\right)=\begin{cases}\frac{1}{8}\left(3-2|r|+\sqrt{1+4|r|-4r^2}\right) & 0\le|r|<1\\ \frac{1}{8}\left(5-2|r|-\sqrt{-7+12|r|-4r^2}\right) & 1\le|r|<2\\ 0 & 2\le|r|\end{cases} \tag{9}$$

ds is the mesh area of the moving boundary. The velocity of the flow field becomes:

$$u_2^{n+1}=u_1^{n+1}+f^2\Delta t \tag{10}$$

Similarly, the Lagrange point velocity of the second iteration is obtained:

$$\hat{\mathrm{u}}_k^2=\sum u_2^{n+1}\cdot\delta(x_k-x)\cdot h^2 \tag{11}$$

The total force on the Lagrange point is

$$F_k^{all}(x_k)=\sum F_k^i(x_k) \tag{12}$$

Then the large eddy model is used to calculate the turbulence model. In the Lattice Boltzmann method, the addition of the large eddy model needs to update the relaxation time, and the total relaxation time is equal to the single relaxation time plus the eddy relaxation time [22].

$$\tau_{total}=\tau+\tau_{sgs} \tag{13}$$

The eddy relaxation time can be calculated by the turbulence viscosity:

$$\tau_{sgs}=\frac{3v_t}{c^2\Delta t} \tag{14}$$

The turbulent eddy viscosity v_t is given by

$$v_t=(C_s\bar{\Delta})^2\sqrt{2\bar{s}_{ij}\bar{s}_{ij}} \tag{15}$$

where the strain-rate tensor $\bar{s}_{ij}$ is related to the non-equilibrium momentum flux tensor by using the Chapman-Enskog expansion.

$$\bar{s}_{ij} = -\frac{3}{2c^2\rho(\tau+\tau_{sgs})\Delta t}\sum_i c_{ik}c_{ij}(f_i - f_i^{eq}) \qquad (16)$$

The method used in this paper has been verified by the flow past a cylinder or a sphere which are the basic and reliable verification methods for fluid mechanics.

B. *Parameter Setting*

The hydrodynamic characteristics of spherical and fish-shaped robots in a long pool will be studied. The pool, as shown in Figure 1, is 5 meters in length, 1.2 meters in width and 0.7 meters in height. The upper and lower boundaries of the pool are set as circulation channels, and the other boundaries are set as no slip boundaries. The fluid is set as water at room temperature, with density ρ equal to $1\times10^3 kg/m^3$ and viscosity v equal to $1\times10^{-6}m^2/s$.

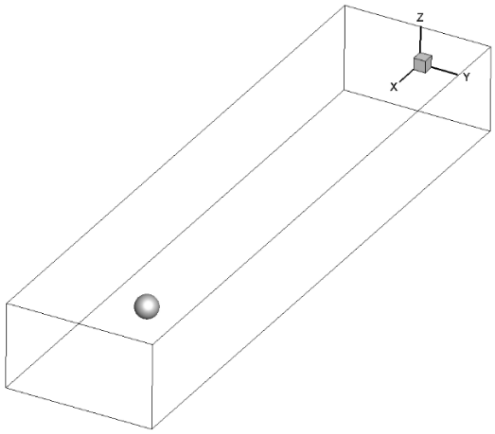

Fig. 1 The computing domain for simulation.

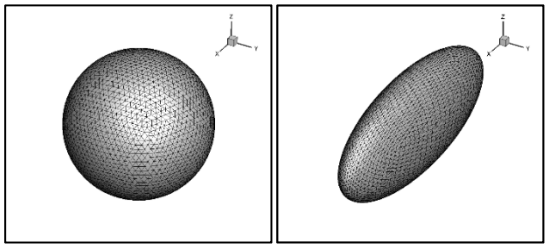

(a) (b)

Fig. 2 The mesh of the spherical and fish-shaped robot models. (a) The spherical robot model. (b) The fish-shaped robot model.

The mesh of the spherical and fish-shaped robot models used in this paper is shown in Figure 2. The meshing accuracy satisfies the calculation condition. In the simulation, the performance of two kinds of robots with the same volume will be compared.

In the experiment, the spherical robot and the fish-shaped robot will be kept the same volume to compare their performance. The length of the fish-shaped robot is controlled in 20-60cm, and the corresponding length of the spherical robot is controlled in 18-40cm. Since the speed of small underwater vehicles is generally low, the speed of the robot are set at 0.05-0.3m/s in a straight line.

III. Simulation and Results

Based on the established immersed boundary lattice Boltzmann model, in this section, the simulation analysis on two kind shapes of robot are conducted. The characteristics of robot motion and the effect are analyzed on flow field. In addition, the influence of the velocity and size of the robot on the flow field and the force of itself is further summarized.

A. *Comparing the velocity characteristics*

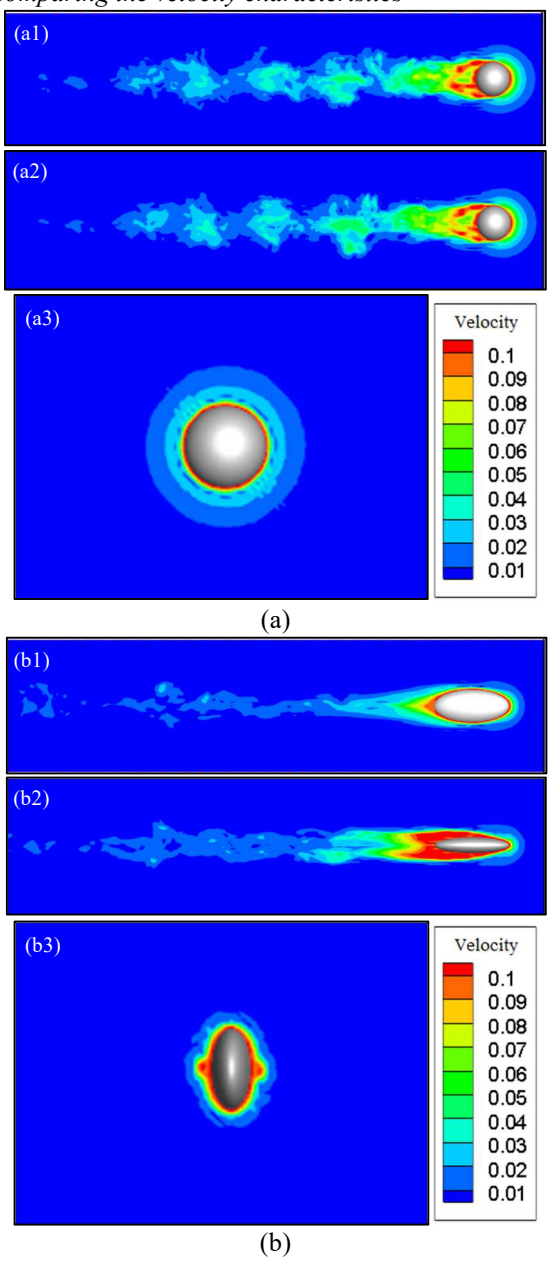

Fig. 3 The velocity of flow field in surge motion of robot (a) spherical robot (b) fish-shaped robot.

In this part, the surge speed of the two robots are set at 0.1m/s. The body length of the fish-shaped robot is 40 cm, and

the body length of the spherical robot is 18.3 cm. Therefore, the volume of the two robots is about 3200 cm^3. The robot moved from one end of the long channel to the other end at a fixed speed (x direction). The snapshot of the robot are taken when it moves steadily to analyze the flow field generated by the robot. FIG. 3 shows the velocity states of the two robots and their flow fields when the time is 10 seconds, where (a) is a spherical robot and (b) is a fish-shaped robot. Figure (a1) and (b1) are the profiles of the XZ plane; (a2) and (b1) are the profiles of the XY plane; (a3) and (b3) are the profiles of the YZ plane. As shown in the Figure 3, (a) and (b) use the same color scale to facilitate comparative analysis. It can be seen from the figure that the wake generated by the spherical robot is larger and has more disturbance to the whole fluid. This may be due to that both types of robots are controlled in the same volume. With the same volume, the spherical robot has a larger inflow area, leading to a larger Reynolds number, so the disturbance is larger.

On the basis of analyzing the velocity of the flow field, the velocity distribution on the surface of the robot is separated, as shown in FIG. 4. In Figure 4, From left to right are the velocity diagram of the XZ, XY and YZ direction sections. The corresponding color bars are listed on the right, and the color scales of Figure 4(a) and Figure4(b) are consistent.

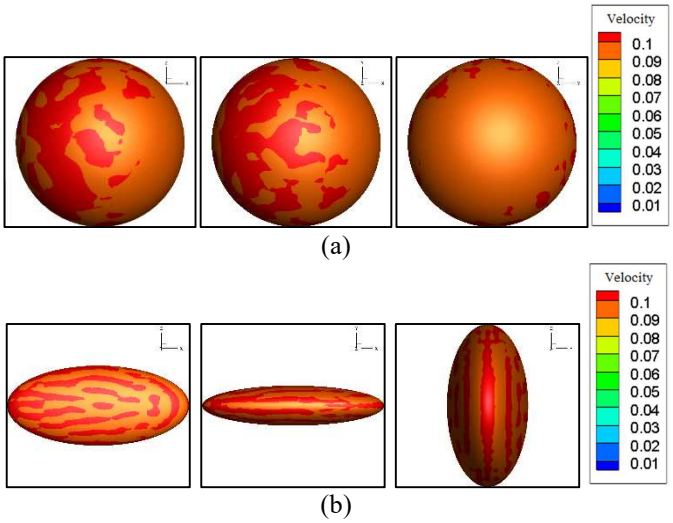

Fig. 4 The distribution of surface velocity on the robot. (a) spherical robot (b) fish-shaped robot.

From the surface velocity distribution of a single robot, the velocity does not change much and is close to the robot's moving velocity. In addition, from the comparison of the surface velocities on the two robots, there is a large area having stability velocity on the spherical robot facing with the flow. Based on this analysis, the speed sensors can be placed on the robot to sense how fast the robot is moving relative to the flow.

The influence caused by robot motion on the flow field has both advantages and disadvantages. On the one hand, this influence will interfere with other robots in the flow field, on the other hand, it is also beneficial to the detection and positioning between robots. Whether it is beneficial or not should be judged according to the practical application of the robots.

B. Comparing the pressure characteristics

Fish sensed the underwater environment through the lateral line system, and then realized hunting and obstacle avoidance. The lateral line system includes velocity sensing parts and pressure sensing parts. In the previous section, the speed effects of two different types of robots have been analyzed. This section will focus on the surface pressure change of the robot caused by the movement of the robot in the static water.

The pressure under water includes static pressure and dynamic pressure. Static pressure is determined by the pressure produced by the water and changes in atmospheric pressure, and dynamic pressure is generated by the robot which moved under water making flow around it. The same simulation conditions are set as that when analyzing the velocity characteristics, and obtained the pressure distribution on the robot surface, as shown in FIG. 5. This figure shows the relative pressure of the robot. Using the pressure value at infinity and the same depth as the baseline, the relative pressure shows the difference between the robot surface pressure and the baseline.

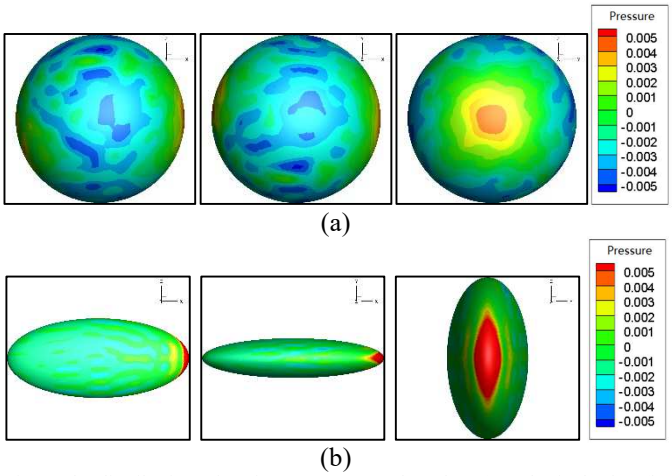

Fig. 5 The distribution of surface pressure on the robot. (a) spherical robot (b) fish-shaped robot.

In Figure 5, From left to right are the pressure diagram of the XZ, XY and YZ direction sections. Figure 5(a) and Figure 5(b) have the same color scale for easy comparison. The pressure distribution varies from -0.005 to 0.001 over the main area of the lateral body of the spherical robot. The pressure distribution varies from -0.003 to 0.001 in the main part of the lateral body of the fish-shaped robot. It can be seen that the pressure distribution of the spherical robot is more uniform, that is, the pressure value on the spherical robot is more widely distributed. In addition, the pressure on the top of the fish-shaped robot will increase sharply, and the increase is more concentrated. The pressure distribution at the top of the spherical robot is relatively uniform.

At present, the research based on artificial lateral line system mainly focused on pressure sensor. Good pressure sensing ability is essential for robots with artificial lateral line

sensing. After the preliminary pressure analysis of the robot moving in still water, it can be considered that the pressure distribution on the surface of the spherical robot is easier to obtain more information of underwater flow. In addition, the spherical robot is more symmetrical and easier to arrange sensor arrays.

C. *The effect of robot velocity on hydrodynamic forces*

The qualitative analysis of hydrodynamic characteristics have been made on moving underwater robot. In the following parts, the further quantitative analysis will be made about the influence of robots' velocity and size on drag resistance force.

Simulations are conducted by moving robot in a long pool, and recording the drag resistance on the robot at each moment. The velocity of robot in each experiment is fixed, the heading of the robot is fixed, and the other states are free. After simulation, the change of drag resistance during the robot movement are gotten, as shown in Figure. 6. In Figure 6, (a) represents the spherical robot, and (b) represents the fish-shaped robot. By comparing the two figures, the force on the fish-shaped robot is more stable than that of the spherical robot. Finally, both robots can achieve stable states.

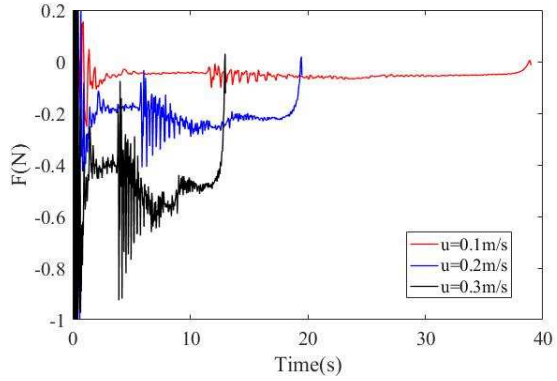

(a)

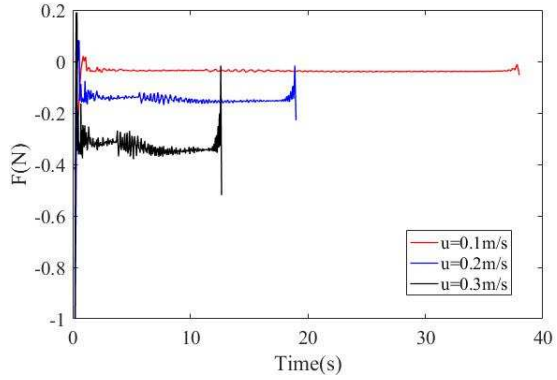

(b)

Fig. 6 The drag resistance force caused by different velocities on the robot. (a) spherical robot (b) fish-shaped robot.

It can also be noticed that the force on the robot fluctuate greatly for a period of time in the process of movement. This may be because the robot began to move at a high speed without excessive process, resulting in a slight oscillation in the flow field. It is believed that the force data in the later half can explain the stability of the robot motion and be used to analyze the motion characteristics of the robot.

TABLE I
THE DRAG RESISTANCE FORCE OF DIFFERENT CONDITIONS

shape	u(m/s)	force(N)
sphere	0.1	0.05387
sphere	0.2	0.2178
sphere	0.3	0.4815
fish	0.1	0.03900
fish	0.2	0.1548
fish	0.3	0.3476

In Table 1, the force values on the robots are listed. It can be seen from the data that the drag resistance is approximately related to the quadratic velocity of the robot.

D. *The effect of robot size on hydrodynamic forces*

In order to explore the influence volume, three levels of robot volume are set, which were marked by the total length of the fish-shaped robot. The volume of these three robots is labelled D=20cm, D=40cm, and D=60cm.

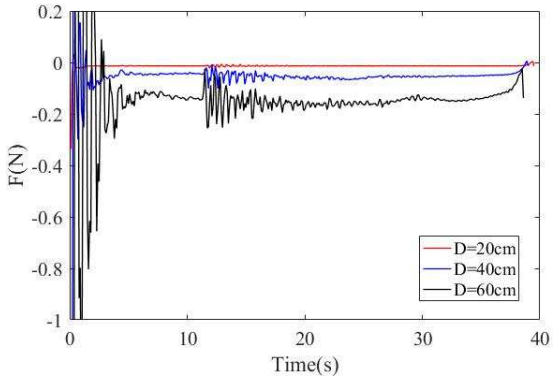

(a)

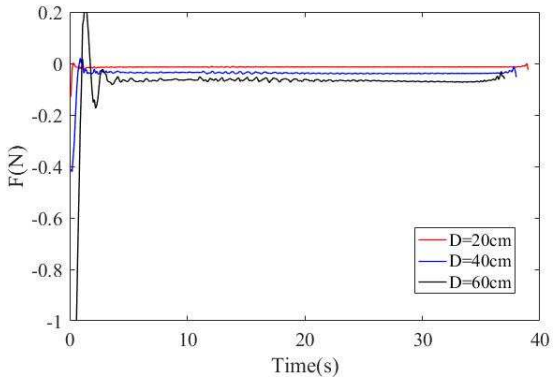

(b)

Fig. 7 The drag resistance force caused by different volume on the robot. (a) spherical robot (b) fish-shaped robot.

The same model is applied to the hydrodynamic simulation, and the results shown in Figure. 7. Figure 7 shows the influence of robot volume change on the drag resistance force of the robot. Similar to the change in velocity, the forces on the spherical robot fluctuate more. In addition, it can be seen

that the volume change has relatively little effect on the drag resistance.

TABLE Ⅱ
THE DRAG RESISTANCE FORCE OF DIFFERENT CONDITIONS

shape	D(cm)	force(N)
sphere	20	0.01339
sphere	40	0.05387
sphere	60	0.1428
fish	20	0.01363
fish	40	0.03900
fish	60	0.06916

In Table Ⅱ, the force values on the robots are listed. It can be seen from the data that the relationship between drag resistance and robot volume is more complicated than a simple proportional relationship.

IV. CONCLUSION

A hydrodynamic model is established to simulate the underwater motion of spherical and fish-shaped robots. Through qualitative and quantitative analysis of hydrodynamic characteristics, the hydrodynamic characteristics of two kinds of shape robots are obtained, which will be applied to guide the underwater sensing and shape design of robots. Firstly, the velocity distribution and surface pressure of the two shape robots are qualitatively analyzed when they move in static water. It can be seen that the spherical robot produces larger wakes and disturbances than the fish-shaped robot. However, the spherical robot has a more uniform surface pressure distribution and perceives a wider range of pressure. Then, the influence of the robot's velocity and volume on the drag resistance are quantitatively analyzed. Both variables have an impact on the drag resistance of the robot, and the impact is different.

ACKNOWLEDGMENT

This work was partly supported by National High Tech. Research and Development Program of China (No.2015AA043202), the National Natural Science Foundation of China (61773064, 61503028), the National Key Research and Development Program of China (No. 2017YFB1304401).

REFERENCES

[1] R. An, S. Guo, Y. Yu, C. Li, and T. Awa, "Task Planning and Collaboration of Jellyfish-inspired Multiple Spherical Underwater Robots," J. Bionic Eng., vol. 19, no. 3, pp. 643–656, 2022, doi: 10.1007/s42235-022-00164-6.

[2] L. Zheng, S. Guo, Y. Piao, S. Gu, and R. An, "Collaboration and Task Planning of Turtle-Inspired Multiple Amphibious Spherical Robots," MICROMACHINES, vol. 11, no. 1, 2020, doi: 10.3390/mi11010071.

[3] S. Guo, S. Cao, and J. Guo, "Study on Decentralization of Spherical Amphibious Multi-robot Control System Based on Smart Contract and Blockchain," J. Bionic Eng., vol. 18, no. 6, pp. 1317–1330, 2021, doi: 10.1007/s42235-021-00073-0.

[4] H. Xing et al., "Design, modeling and control of a miniature bio-inspired amphibious spherical robot," MECHATRONICS, vol. 77, 2021, doi: 10.1016/j.mechatronics.2021.102574.

[5] H. Xing, S. Guo, L. Shi, X. Hou, Y. Liu, and H. Liu, "Design, modeling and experimental evaluation of a legged, multi-vectored water-jet composite driving mechanism for an amphibious spherical robot," Microsyst. Technol. Nanosyst. STORAGE Process. Syst., vol. 26, no. 2, pp. 475–487, 2020, doi: 10.1007/s00542-019-04536-7.

[6] Y. Zhai, X. Zheng, and G. Xie, "Fish Lateral Line Inspired Flow Sensors and Flow-aided Control: A Review," J. Bionic Eng., vol. 18, no. 2, pp. 264–291, 2021, doi: 10.1007/s42235-021-0034-y.

[7] X. Zheng, A. M. Kamat, M. Cao, and A. G. P. Kottapalli, "Creating underwater vision through wavy whiskers: a review of the flow-sensing mechanisms and biomimetic potential of seal whiskers," J. R. Soc. INTERFACE, vol. 18, no. 183, 2021, doi: 10.1098/rsif.2021.0629.

[8] A. Sahoo, S. K. Dwivedy, and P. S. Robi, "Advancements in the field of autonomous underwater vehicle," Ocean Eng., vol. 181, pp. 145–160, 2019, doi: 10.1016/j.oceaneng.2019.04.011.

[9] X. Hou et al., "Hydrodynamic Analysis-Based Modeling and Experimental Verification of a New Water-Jet Thruster for an Amphibious Spherical Robot," SENSORS, vol. 19, no. 2, 2019, doi: 10.3390/s19020259.

[10] Y.-Z. Chen et al., "Numerical Simulation of Hydrodynamic Characteristics of Underwater Hull Cleaning Robot Using CFD Techniques," J. Sh. Res., vol. 64, no. 1, pp. 1–22, 2020, doi: 10.5957/jsr.2020.64.1.1.

[11] M. Marcin, S. Adam, Z. Jerzy, and M. Marcin, "Fish-like shaped robot for underwater surveillance and reconnaissance - Hull design and study of drag and noise," Ocean Eng., vol. 217, 2020, doi: 10.1016/j.oceaneng.2020.107889.

[12] A. Honaryar and M. Ghiasi, "Design of a Bio-inspired Hull Shape for an AUV from Hydrodynamic Stability Point of View through Experiment and Numerical Analysis," J. Bionic Eng., vol. 15, no. 6, pp. 950–959, 2018, doi: 10.1007/s42235-018-0083-z.

[13] S. Gu, S. Guo, and L. Zheng, "A highly stable and efficient spherical underwater robot with hybrid propulsion devices," Auton. Robots, vol. 44, no. 5, pp. 759–771, 2020, doi: 10.1007/s10514-019-09895-8.

[14] H. Xing et al., "A Multi-Sensor Fusion Self-Localization System of a Miniature Underwater Robot in Structured and GPS-Denied Environments," IEEE Sens. J., vol. 21, no. 23, pp. 27136–27146, 2021, doi: 10.1109/JSEN.2021.3120663.

[15] Z. Zhou, J. Liu, and J. Yu, "A Survey of Underwater Multi-Robot Systems," IEEE-CAA J. Autom. Sin., vol. 9, no. 1, pp. 1–18, 2022, doi: 10.1109/JAS.2021.1004269.

[16] X. Hou et al., "Improved Model Predictive-Based Underwater Trajectory Tracking Control for the Biomimetic Spherical Robot under Constraints," Appl. Sci., vol. 10, no. 22, 2020, doi: 10.3390/app10228106.

[17] R. An, S. Guo, Y. Yu, C. Li, and T. Awa, "Multiple Bio-Inspired Father-Son Underwater Robot for Underwater Target Object Acquisition and Identification," MICROMACHINES, vol. 13, no. 1, 2022, doi: 10.3390/mi13010025.

[18] W. Niu, S. Wang, Y. Wang, Y. Song, and Y. Zhu, "Stability Analysis of Hybrid-Driven Underwater Glider," CHINA Ocean Eng., vol. 31, no. 5, pp. 528–538, 2017, doi: 10.1007/s13344-017-0061-y.

[19] C.-W. Chen et al., "Computational fluid dynamics study of the motion stability of an autonomous underwater helicopter," Ocean Eng., vol. 143, pp. 227–239, 2017, doi: 10.1016/j.oceaneng.2017.07.020.

[20] W. Zhong, A. Yu, X. Liu, Z. Tong, and H. Zhang, "DEM/CFD-DEM Modelling of Non-spherical Particulate Systems: Theoretical Developments and Applications," POWDER Technol., vol. 302, pp. 108–152, 2016, doi: 10.1016/j.powtec.2016.07.010.

[21] W. Zhong, A. Yu, G. Zhou, J. Xie, and H. Zhang, "CFD simulation of dense particulate reaction system: Approaches, recent advances and applications," Chem. Eng. Sci., vol. 140, pp. 16–43, 2016, doi: 10.1016/j.ces.2015.09.035.

[22] S. T. Bose and G. I. Park, "Wall-Modeled Large-Eddy Simulation for Complex Turbulent Flows," in ANNUAL REVIEW OF FLUID MECHANICS, VOL 50, vol. 50, S. H. Davis and P. Moin, Eds. 4139 EL CAMINO WAY, PO BOX 10139, PALO ALTO, CA 94303-0897 USA: ANNUAL REVIEWS, 2018, pp. 535–561.